JOURNAL OF PROPULSION AND POWER
Vol. 9, No. 2, March–April 1993

Numerical Modeling of Wall-Injected Scramjet Experiments

C. P. Brescianini* and R. G. Morgan†
University of Queensland, Brisbane, Queensland, Australia

A wall-injected, hydrogen-fueled scramjet is modeled numerically using a parabolic Navier-Stokes computer code with a k-ε turbulence model and finite-rate chemistry. The numerical results are compared to experimental scramjet data taken in a shock tunnel and are found to be in reasonable agreement. At the conditions studied, the numerical results show that combustion in the scramjet is mainly mixing limited.

Nomenclature

C_μ, $C_{\varepsilon 1}$, $C_{\varepsilon 2}$ = constant coefficients appearing in turbulence model
E = constant in Logarithmic Law of the Wall
F_A = constant used to estimate background turbulence
H = stagnation enthalpy
H_j = fuel injector step height
K = hydrogen injector flow rate constant
k = kinetic energy of turbulence
l_ε = dissipation length scale
M = Mach number
m_{NO}, m_O = mass fractions of species NO and O, respectively
$\dot{m}$ = mass flow rate
P_H = integration constant in energy wall function
p = pressure
$\dot{q}$ = heat transfer rate
S_H = near-wall Stanton number, $-\dot{q}_w/(H_{aw} - H_w)_c(\rho u)_c$
St = Stanton number based on inlet conditions, $-\dot{q}_w/(H_{aw} - H_w)_i(\rho u)_i$
s = shear stress coefficient, $\tau_w/(\rho u^2)_c$
T = temperature
U_{sh} = incident shock speed
u = axial velocity
v = transverse velocity
x = axial distance measured from injector
y = transverse distance
γ = ratio of specific heats
η_{MIX} = mixing efficiency; amount of reacted hydrogen (hydrogen mass in the form of water) if all mixed hydrogen and oxygen reacted completely, divided by the same quantity if mixing had been complete
η_{RR} = reaction-rate combustion efficiency, reacted hydrogen divided by the amount of reacted hydrogen if the hydrogen and oxygen which are mixed reacted completely
η_{STOICH} = stoichiometric combustion efficiency, $\eta_{MIX}X\eta_{RR}$
η_{TF} = total fuel combustion efficiency; reacted hydrogen, divided by the total amount of hydrogen
κ = von Karman's constant
μ = viscosity
ρ = density
σ_H = Prandtl number
τ = shear stress
ϕ = equivalence ratio

Subscripts
aw = adiabatic wall
c = near-wall grid point
$H2$ = hydrogen
i = inlet
j = injector
l = laminar
S = stagnation
t = turbulent
w = wall

Superscript
$+$ = Law of the Wall variable

Received Dec. 21, 1990; revision received July 1, 1992; accepted for publication Aug. 28, 1992.

*Graduate Student, Department of Mechanical Engineering. Student Member AIAA.
†Senior Lecturer, Department of Mechanical Engineering. Member AIAA.

Introduction

MOST of the high-speed air-breathing propulsion research for the National Aero-Space Plane (NASP) has centered around the scramjet engine. Ground-testing of such an engine requires a wind-tunnel facility which cannot only produce supersonic gas flow of the correct Mach number, but also the high temperatures and pressures needed to simulate the combustion process. The only types of facilities currently available for performing these simulations, at stagnation enthalpies greater than 3.5 MJ/kg (corresponding to flight speeds >2.7 km/s) are pulsed facilities.

To avoid the need for exposing a fuel injection strut to a high-speed airflow, fuel injection from the wall of the scramjet is likely to be used. To test the wall-injected scramjet at high-enthalpy test conditions, a series of shock-tunnel experiments were performed by Morgan et al.[1,2] These experiments indicated static-pressure rises in the combustion chamber which were significantly below what had been expected. The pressures rises were taken as indicative of the amount of combustion which had occurred. In an attempt to explain the poor combustion, the authors of Refs. 1 and 2 postulated the existence of a significant layer of cold hydrogen and air located along the lower wall of the scramjet model. It was presumed that this layer had been quenched by the cold walls of the model to below the temperature required for ignition and combustion. It was a very difficult problem to measure the gas temperature in a shock-tunnel flow so that the theory of a quenched layer could be confirmed. As an alternative approach, it was decided to carry out a detailed numerical study of the scramjet flow using a computational fluid dynamics (CFD) code. By examining the numerical results, it was hoped that the reasons for the low static-pressure rises could be identified, and that the suggestion of a quenched layer of fuel could be examined in more detail.

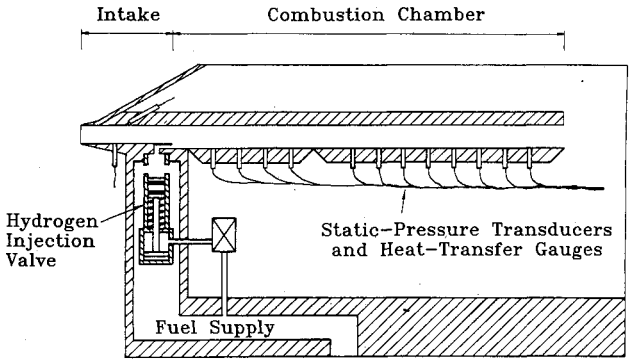

Fig. 1 Schematic of wall-injected scramjet model.

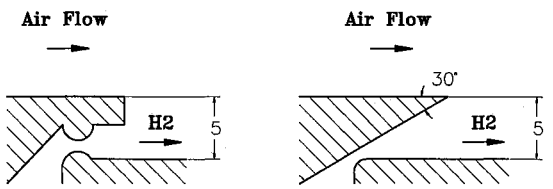

a) Cylindrical injector b) Source-flow injector

Fig. 2 Hydrogen wall injectors.

Description of Wall-Injected Scramjet Model

The wall-injected scramjet model used in Refs. 1 and 2 is depicted in Fig. 1. The model consisted of a 20-mm-high by 51-mm-wide inlet, followed by a 5-mm step along the lower wall, 88.5-mm downstream of the model's inlet. The aspect ratio of the injector was approximately 10:1, which was thought sufficient to create nominally two-dimensional fuel/air mixing. Hydrogen fuel (with total temperature equal to room temperature) was injected from the rear of this step into a constant-area combustion chamber. Two types of nozzles were used in the wall injector to meter the flow of hydrogen. Details of these two nozzles can be seen in Figs. 2a and 2b. The flow of hydrogen through the nozzles was varied by changing the hydrogen injection (reservoir) pressure.

Experimental data consisted of static-pressure measurements at the inlet of the scramjet and along the lower wall of the combustion chamber, as well as heat transfer measurements along the lower wall. The final transducer in the combustion chamber (a heat transfer gauge) was located 316-mm downstream of the injector.

The high-enthalpy test gas for the experiments was provided by the T3 free-piston-driven shock tunnel (Stalker[3]) which was operated in reflected, undertailored mode. Typical test times were of the order 0.5–1.0 ms. The test gas was expanded from the stagnation conditions at the end of the shock tube, to the freestream test conditions, by a nominally Mach 3.5, contoured, axisymmetric nozzle.

Numerical Modeling

Accurate modeling of all aspects of the short-duration experiment, including the flow-establishment time, required a time-accurate computer code capable of solving the complete Navier-Stokes equations. Time-dependent simulations of similar flows have been performed by Rogers and Weidner[4,5] and Jacobs et al.,[6] however, the computational effort required was so large that the solutions were limited to nonreacting cases where the turbulent mixing effects were usually ignored. In the present study, numerical simulations of the scramjet flow were performed using a two-dimensional, steady, parabolic Navier-Stokes code where the effects of chemistry and turbulence were included. The steady-state/transient-flow comparisons performed in Refs. 4–6 (keeping in mind the limited flows studied to date) indicate that the steady-state solutions should provide good approximations to the experiments.

Previous steady-state computations of the wall-injected scramjet experiments have been performed by Rogers et al.[7] The results presented here go further than this earlier work by including finite-rate chemical reactions, compressible wall functions, and a re-evaluation of the experimental data.

Description of Computer Program

Solution Technique

Numerical simulations of the scramjet flow were performed by solving partial differential equations for the transport of x and y momentum, energy, and species. The partial differential equations which were solved were the same as those given by Elghobashi and Spalding,[8] and the solution was accomplished by the control volume-based finite-difference method of Patankar and Spalding.[9] The effects of lateral pressure gradients in the flow were included by using the SIMPLE algorithm, as described in Ref. 8. The turbulent viscosity was evaluated using a k-ε model of turbulence, along with the "standard" model constants, as recommended by Launder and Spalding.[10]

Wall Functions

The fluxes of heat and shear stress to the scramjet walls were evaluated by using wall functions. The wall functions assumed that the Logarithmic Law of the Wall

$$u^+ = (1/\kappa)\, \ell_n\, (Ey^+) \tag{1}$$

held in the fully turbulent region close to the wall. The variables u^+ and y^+ were defined by

$$u^+ = (u_{\text{eff}}/\sqrt{\tau_w/\rho_w}) \tag{2}$$

$$y^+ = (y_c\sqrt{\tau_w\rho_w}/\mu_w) \tag{3}$$

where u_{eff} was the van Driest effective velocity[11] given by

$$u_{\text{eff}} = \int_{u=0}^{u=u_c} \sqrt{\rho/\rho_w}\, du \tag{4}$$

The Law of the Wall has generally been found to be applicable in cases with pressure gradients, and consequently Eq. (1) was not altered to account for the pressure gradients present in the scramjet flow. The values assigned to the constants κ and E were 0.435 and 9.00, respectively. These values have been previously suggested by Patankar and Spalding.[9] The integration required in Eq. (4) was carried out numerically, and the density ratio was evaluated by using the modified Crocco-Busemann relation[12] along with the ideal-gas relation.

The values of k and ε at the near-wall grid points were evaluated from the usual assumption of equilibrium turbulence, which results in the following expressions:

$$k_c = (\tau_{t,c}/\sqrt{C_\mu}\rho_c) \tag{5}$$

$$\varepsilon_c = (C_\mu^{0.75}k_c^{1.5}/\kappa y_c) \tag{6}$$

The shear stress at the near-wall grid point was approximated by

$$\tau_c = \tau_w + y_c \frac{dp}{dx} \tag{7}$$

The heat transfer at the walls was evaluated by making use of the following wall function:

$$S_H = s/[\sigma_H(\tau_w/\tau_*) + P_H\sqrt{s}\sqrt{\rho_c/\rho_w}] \quad (8)$$

where

$$\tau_* = \left[u_c \Big/ \int_{u=0}^{u=u_c} (1/\tau)\, du\right] \quad (9)$$

This equation was based on the wall-function relation given by Spalding,[13] except that it was modified here to account for the variation in fluid properties and shear stress throughout the near-wall layer. Catalytic-wall effects were assumed negligible. The value for P_H was determined by using the relationship given by Jayatillaka.[14]

Chemistry

The hydrogen/air chemistry was evaluated by assuming that nitrogen was inert, and using an 8-reaction, 7-species, finite-rate chemistry scheme described by Evans and Schexnayder.[15] Evans and Schexnayder examined several supersonic combustion test cases and found that the eight-reaction mechanism was as good as a larger 25-reaction mechanism once ignition had occurred.

Experimental Test Conditions

Computational results are presented for two nominal test conditions reported in Ref. 2. The experimental data was sampled at intervals of 0.016 ms, with typically at least 100 samples being recorded for each transducer. All the experimental pressures presented here have been time-averaged over 0.08 ms to help eliminate noise.

The heat transfer measurements were taken using thin-film heat transfer gauges. The gauges measured the temperature of a thin film of platinum, painted onto a substrate of Down Corning "Macor®" glass ceramic. The variation in temperature with time was then integrated to obtain the heat transfer rate into the substrate using the one-dimensional, semi-finite theory of Schultz and Jones.[16] A value of 2000 $Jm^{-2}K^{-1}s^{-1/2}$ was used as the thermal product of the substrate during the analysis.

The stagnation temperature of the test gas in the shock tube was evaluated using a one-dimensional, equilibrium chemistry computer program known as ESTC.[17] The program used the shock-tube filling pressure, temperature, and experimentally-measured incident shock speed to determine the conditions behind the reflected shock at the end of the shock tube. The program then let the test gas expand isentropically to the measured stagnation pressure during the test time. The final results are indicated in Table 1.

The flow conditions at the exit of the shock-tunnel nozzle (and thus at the inlet to the scramjet) were then estimated by using a quasi-one-dimensional nozzle flow program, known as NENZF.[18] NENZF took into consideration the nonequilibrium chemical effects which occurred in the shock-tunnel nozzle as the test gas expanded from stagnation to freestream test conditions. The one-dimensional nature of the computation, however, did not allow for boundary-layer growth in the nozzle or the true two-dimensional nature of the pressure field. A first-order correction was made by terminating computations when the predicted static pressure agreed closely with the experimentally recorded static pressure at the inlet to the scramjet. The results are shown in Table 2.

The experimentally recorded hydrogen reservoir pressures, and the type of hydrogen injection nozzles used, are shown in Table 3. The mass-flow rate through the injector was calculated from the formula

$$\dot{m}_{H2} = Kp_{s,H2} \quad (10)$$

where the value of K was determined experimentally to be 3.2×10^{-5} kg/s/kPa for the cylindrical injector. An identical value of K has been assumed here for the source-flow injector, which had a nominally identical throat size.

The equivalence ratio was then calculated using this hydrogen flow rate and an airflow rate evaluated from the conditions shown in Table 2. The results are included in Table 3.

Initial Conditions for Computations

Numerical computations began at the point of hydrogen injection, and marched downstream. The flow region immediately behind the lip of the cylindrical injector could not be modeled with the parabolic Navier-Stokes code used during the present analysis, and therefore, the initial hydrogen flow was assumed to have fully expanded to the injector step height. Since nominally identical experimental results are also presented which use the source-flow injector (which had a very thin trailing edge), this approach was thought justified.

Table 1 Conditions in shock tube

Run no.	Test condition	Test gas	Initial shock-tube pressure, kPa	U_{sh}, m/s	P_s, MPa	T_s, K
7241	A	Air	150	2180	13.9	3120
7281	A	Air	150	2070	12.5	2880
7247	B	Air	54	2980	10.9	4730
7279	B	Air	54	2980	13.9	4900

[a]Initial shock tube temperature = 296K.

Table 2 Scramjet inlet conditions

Run no.	H,[a,b] MJ/kg	T_i, K	p_i, kPa	ρ_i, kg/m^3	u_i, m/s	M_i	m_0	m_{NO}	γ_i
7241	3.9	1080	148	0.478	2240	3.5	0.0003	0.0739	1.33
7281	3.5	1030	143	0.487	2170	3.5	0.0002	0.0268	1.34
7247	7.4	2220	147	0.228	2970	3.3	0.0164	0.0657	1.30
7279	7.7	2340	184	0.270	3040	3.2	0.0162	0.0653	1.30

[a]H = 0.3 MJ/kg for air at 300 K. [b]H is evaluated at the stagnation conditions in the shock tube.

Table 3 Hydrogen injection conditions and turbulence constants

Run no.	$p_{S,H2}$, kPa	ϕ	Inject nozzle	l_e/H_j	F_A, $\times 10^{-4}$	$\sigma_{H,t}$	$\sigma_{H,i}$
7241	993	1.0	cylindrical	0.060	4.0	0.9	0.72
7281	927	1.0	source				
7247	993	1.6	cylindrical	0.003	4.0	0.8	0.72
7279	1010	1.3	source				

The experimental results for the two types of injectors could not be distinguished within the experimental accuracy of the shock-tunnel data.

The airstream conditions at the initial station were taken as being identical to those at the scramjet inlet (Table 2), except for the addition of a small boundary layer on the upper wall. A step change in the velocity, temperature, pressure, and species concentrations was assumed at the hydrogen/air interface, and the initial hydrogen fuel was assumed to be moving parallel to the main airflow. The wall temperature was assumed fixed at 300 K.

The calculated test-gas composition indicated that a substantial part of the dissociated oxygen was in the form of NO (see Table 2). Since the combustion model used in the calculations did not consider the species NO, the components of NO were added to the concentrations of O_2 and N_2. No adjustments were made to the mixture temperature.

The initial values of turbulent kinetic energy and dissipation were estimated from

$$k = \max\left[\left(\frac{l_\varepsilon}{\sqrt{C_\mu}}\frac{\partial u}{\partial y}\right)^2,\ F_A u^2\right] \tag{11}$$

$$\varepsilon = \frac{C_\mu k^{3/2}}{l_\varepsilon} \tag{12}$$

Equation (11) was based on an assumption of equilibrium turbulence in the regions of turbulence production. The dissipation length scale l_ε, required in Eqs. (11) and (12), was adjusted until reasonable agreement was obtained with the computed and experimental heat-transfer results immediately downstream of the injector. The final values of l_ε and F_A selected are indicated in Table 3. Although adjustment of the initial length scale in this way was obviously not completely satisfactory, it must be viewed in the context of the uncertainty in the inlet conditions. Adjustment of the length scale was found to affect the heat transfer near the injector, however, further downstream, the heat transfer and pressure distributions were relatively insensitive to the chosen length scale.

The Prandtl numbers used during the computations are also indicated in Table 3. A Lewis number of unity was assumed.

Numerical Results

H = 3.9 MJ/kg, ϕ = 1.0

Figure 3a shows the computed static pressures along the lower wall of the scramjet for run 7241. Also shown on Fig. 3a are the experimental results obtained using the cylindrical (run 7241) and the source-flow (run 7281) hydrogen-injection nozzles. The overall pressure level predicted by the computer program is in good agreement with the experiments, although the agreement in the pressure distribution shape is not as good. The widely spaced pressure transducers provide only coarse axial resolution, and it is difficult to make out the exact shape of the experimental pressure variation. The large troughs in the computed pressures are due to the initial mismatch in the airstream and fuel stream static pressures which results in a strong shock/expansion structure downstream of the injector. The large troughs apparent in the computed profile appear to be missing in the experimental results. This may be due to the lack of resolution, or it may also indicate that the modeling of the initial conditions at the injector needs improving. The experimentally recorded hydrogen reservoir pressures may also be too low, as these were measured in quite a small plenum chamber located upstream of the injector. A higher stagnation pressure would reduce the strength of the shock and expansion waves.

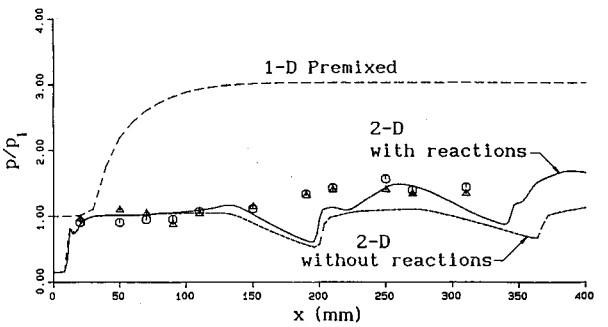

a) Normalized static pressure along lower wall

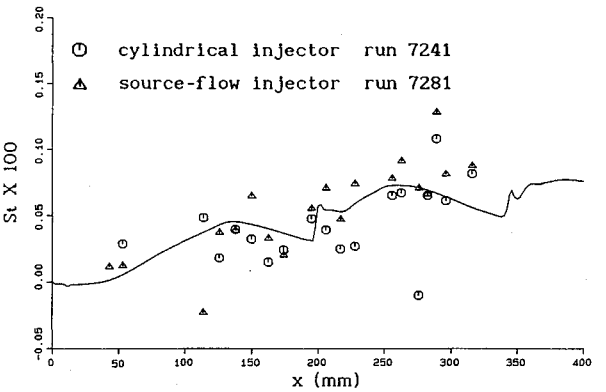

b) Stanton number along lower wall

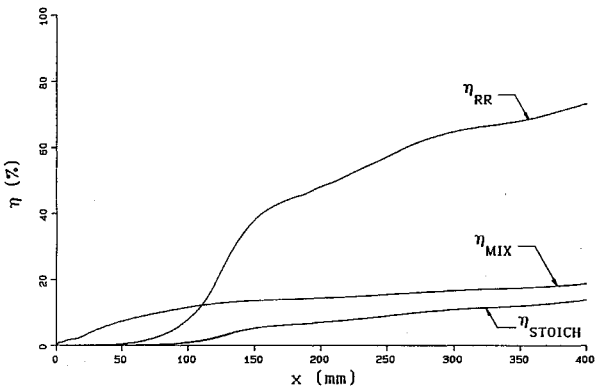

c) Combustion and mixing efficiencies

Fig. 3 Variations along scramjet; run 7241; H = 3.9 MJ/kg.

The predicted wave structure downstream of the injector can easily be seen in Fig. 4a, which is a contour map of static pressure normalized by the airstream inlet pressure. On the contour map the flow is traveling from left to right, with hydrogen injection at the lower left corner. The vertical scale has been expanded to allow easier analysis of the results.

Figure 3a includes the predicted pressures if chemical reactions are ignored during the computations. The results obtained when chemical reactions are considered are in closer agreement with the experiments. Also included on Fig. 3a is the axial variation in pressure obtained from a one-dimensional code (Bittker and Scullin[19]) where the hydrogen and air gases were assumed perfectly mixed to the same equivalence ratio as the experiments. The initial conditions for these computations were identical to the airstream conditions given in Table 2, and no alterations were made to account for the change in energy and momentum as the hydrogen and airstreams mix. The chemical reaction scheme chosen was the same as the eight-reaction scheme used for the two-dimensional calculation. The one-dimensional results give some indication that a noticeable ignition delay can be expected. The

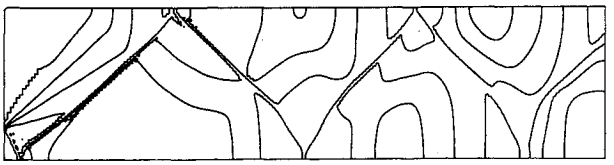

a) Normalized static pressure (p/p_i); contour step = 0.20

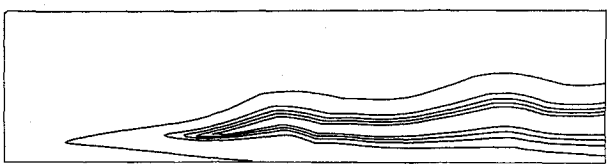

b) H_2O mass fraction; contour step = 0.05

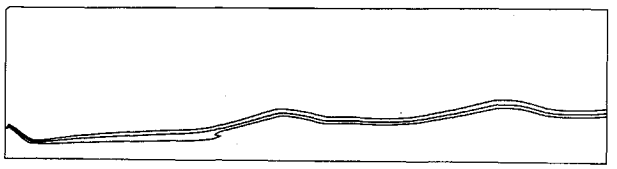

c) Local equivalence ratio; ϕ = 0.2, 1.0, 5.0

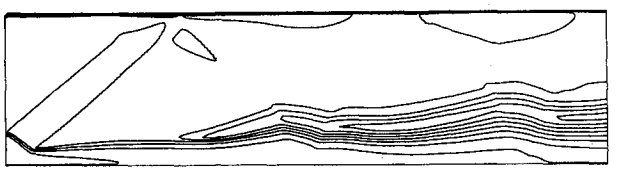

d) Static temperature (T) (T_w = 300 K); contour step = 250 K

Fig. 4 Computed contour maps; run 7241.

one-dimensional results also display the significantly higher pressure rise which would be expected if mixing was complete. The fact that the experiments and the predicted pressures from the two-dimensional computation are so much lower than the one-dimensional theory would indicate that the heat release is mixing controlled under these conditions.

Figure 3b compares experimental and computed Stanton numbers along the lower wall of the scramjet. The experimental Stanton numbers have been obtained by normalizing the experimental heat transfer data with the theoretical inlet test conditions shown in Table 2, and using a recovery factor of 0.9. There is quite a large amount of scatter in the experimental data and the exact shape of the heat transfer distribution is not clear, however, the computed results appear to agree satisfactorily. Within the experimental accuracy, the heat-transfer rates show no significant difference between injector types.

Figure 4b shows contours of water mass fraction. No significant water is produced until approximately 40-mm downstream of injection. This is in approximate agreement with the ignition delay indicated by the one-dimensional calculation in Fig. 1a.

According to Huber et al.,[20] self-ignition may be expected to occur in regions where the local mixture equivalence ratio is approximately 0.2 and the temperatures are above 800 K. Local equivalence-ratio contours of 0.2, 1.0, and 5.0 are displayed in Fig. 4c, while static-temperature contours are shown in Fig. 4d. A significant region of cold gas can be seen near the lower wall in Fig. 4d, however, this cold region is the result of the large amount of injected cold hydrogen, rather than due to significant heat loss through the walls. By comparing Figs. 4c and 4d, the combustion region can be seen to spread out into the hot airstream. The spreading rate is slow, however, with the combustion region not even reaching the halfway point across the flow by the end of the duct.

Combustion and mixing efficiencies are shown in Fig. 3c. η_{RR} is seen to be large once ignition has occurred. The finite-rate chemistry limits the combustion by only a small extent. On the other hand, η_{MIX} is very poor, reaching only 19% by the end of the duct. As a result of the poor mixing, the overall combustion efficiencies, as measured by η_{STOICH} and η_{TF} (which are identical if $\phi \leq 1$), remain small.

H = 7.4 MJ/kg, ϕ = 1.6

Figure 5a shows the computed pressure variation along the lower wall of the scramjet at the higher enthalpy condition, corresponding to run 7247. Two experimental results are again shown; one using the cylindrical injector (run 7247, ϕ = 1.6), and the other the source-flow injector (run 7279, ϕ = 1.3). Both the shape and the overall pressure level measured at the end of the duct appear to be reasonably well-predicted.

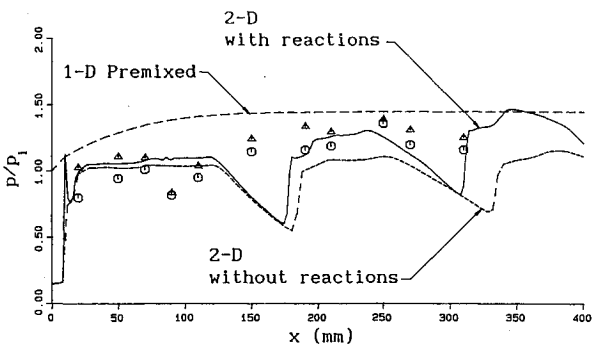

a) Normalized static pressure along lower wall

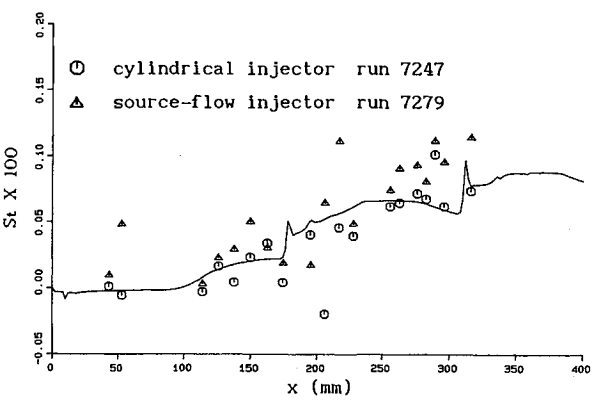

b) Stanton number along lower wall

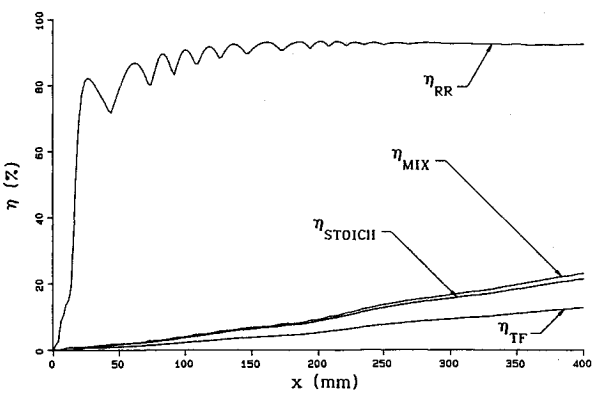

c) Combustion and mixing efficiencies

Fig. 5 Variations along scramjet; run 7247; H = 7.4 MG/kg.

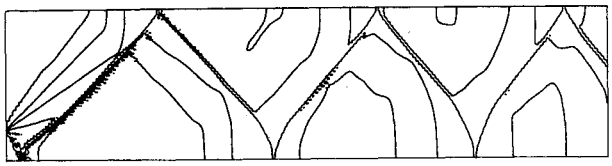

a) Normalized static pressure (p/p_i); contour step = 0.20

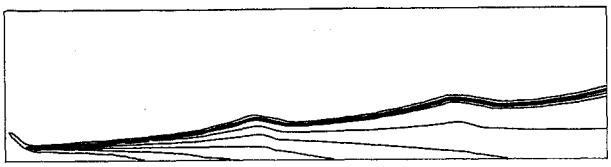

b) H_2O mass fraction; contour step = 0.05

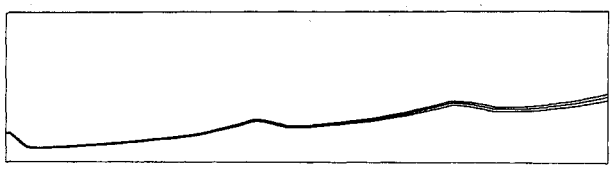

c) Local equivalence ratio; ϕ = 0.2, 1.0, 5.0

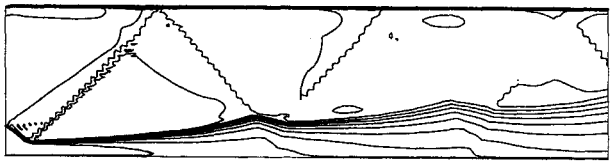

d) Static temperature (T) (T_w = 300 K); contour step = 250K

Fig. 6 Computed contour maps; run 7247.

The main source of the large predicted pressure waves is again the mismatch in the initial hydrogen/air static pressures. The low axial-distance resolution in the pressure measurements again makes it difficult to determine whether such a pressure wave is present in the experimental results. A significant pressure rise due to combustion is also present in the results. This can be seen by the noticeable difference between the pressure profiles obtained when the program is used with and without the chemical reactions.

The one-dimensional calculations, also shown on Fig. 5a, predict almost immediate ignition. The ignition process is no doubt aided by the high test-gas temperatures, and the large fraction of dissociated oxygen initially present in the flow. By the end of the duct, the pressure level predicted by the two-dimensional calculation approaches that of the ideal one-dimensional case.

The Stanton-number predictions, shown in Fig. 5b, agree quite well with the two sets of experimental data. The predictions are in slightly closer agreement with the results for run 7247, which were used as the initial conditions for the computations.

Water contours (Fig. 6b) show that almost immediate ignition is predicted after injection. This agrees with the one-dimensional calculations shown in Fig. 5a.

The local-equivalence ratio contours (Fig. 6c) and temperature contours (Fig. 6d) show a very thin flame front spreading out into the hot airstream. The flame front is located well away from any cold gas located near the walls.

Figure 5c shows that 93% of the mixed hydrogen has reacted (η_{RR}), however, the η_{MIX} is again very low. As a result, only 22% of the total hydrogen available for reaction has been converted to water (η_{STOICH}).

Conclusions

Numerical simulations of high-enthalpy, wall-injected scramjet experiments have been presented. The numerical results for the lower-enthalpy condition show reasonable agreement with experiment. The computed results show a significant ignition delay and a low fuel/air mixing rate.

The numerical results for the higher enthalpy condition show good static pressure and heat transfer predictions when compared to the shock-tunnel data. The numerical results indicate almost immediate ignition, but also a low mixing rate.

For both enthalpy conditions, the predicted flame front spread outwards into the hot airstream. A layer of cold gas was found to be present near the lower walls of the scramjet model, however, this cool layer was the result of the large amount of injected cold hydrogen which had not reacted or significantly mixed with the airstream, rather than due to cold model walls. The computations indicated that the main combustion-limiting factor, after ignition had occurred, was the rate at which the hydrogen mixed with the airstream. Wall quenching appeared not to be a problem.

Acknowledgments

This work was supported by grants from the Australian Research Council and the NASA Langley Research Center, Hypersonic Propulsion Branch, through NASA Grant NAGW-674. The authors are grateful to Ray Stalker for many discussions concerning the analysis of the shock-tunnel data taken in T3.

References

[1]Morgan, R. G., Paull, A., Morris, N., and Stalker, R. J., "Scramjet Sidewall Burning—Preliminary Shock Tunnel Results," Dept. of Mechanical Engineering, Univ. of Queensland, Research Rept. 12/85, NASA Contract NAGW 674, Brisbane, Queensland, Australia, 1985.

[2]Morgan, R. G., Paull, A., Morris, N., and Stalker, R. J., "Further Shock Tunnel Studies of Scramjet Phenomena," Dept. of Mechanical Engineering, Univ. of Queensland, Research Rept. 10/86, NASA Contract NAGW-674, Brisbane, Queensland, Australia, 1986.

[3]Stalker, R. J., "Development of a Hypervelocity Wind Tunnel," *Aeronautical Journal of the Royal Aeronautical Society*, Vol. 76, June 1972, pp. 374–384.

[4]Rogers, R. C., and Weidner, E. H., "Numerical Analysis of Pulse Facility Transient Flow Through a Supersonic Combustor Model," AIAA Paper 88-3261, July 1988.

[5]Rogers, R. C., and Weidner, E. H., "Scramjet Mixing Establishment Times for a Pulse Facility," AIAA Paper 91-0229, Jan. 1991.

[6]Jacobs, P. A., Rogers, R. C., Weidner, E. H., and Bittner, R. D., "Flow Establishment in a Generic Scramjet Combustor," AIAA Paper 90-2096, July 1990.

[7]Rogers, C. R., Drummond, J. P., and Weidner, E. H., "Numerical Analysis of Shock Tunnel Data for Hydrogen Injection into Supersonic Air Flows," 24th JANNAF Combustion Meeting, Monterey, CA, Oct. 1987.

[8]Elghobashi, S., and Spalding, D. B., "Equilibrium Chemical Reaction of Supersonic Hydrogen-Air Jets (The ALMA Computer Program)," NASA CR-2725, Jan. 1977.

[9]Patankar, S. V., and Spalding, D. B., *Heat and Mass Transfer in Boundary Layers*, 2nd ed., International Textbook, London, 1970.

[10]Launder, B. E., and Spalding, D. B., "The Numerical Computation of Turbulent Flows," *Computer Methods in Applied Mechanics and Engineering*, Vol. 3, 1974, pp. 269–289.

[11]van Driest, E. R., "Turbulent Boundary Layers in Compressible Fluids," *Journal of the Aeronautical Sciences*, Vol. 18, No. 3, 1951, pp. 145–160.

[12]White, F. M., *Viscous Fluid Flow*, McGraw-Hill, New York, 1974, p. 627.

[13]Spalding, D. B. "GENMIX—A General Computer Program for Two-Dimensional Parabolic Phenomena," Pergamon, Oxford, England, UK, 1977.

[14]Jayatillaka, C. V. L., "The Influence of Prandtl Number and Surface Roughness on the Resistance of the Laminar Sub-Layer to

Momentum and Heat Transfer," *Progress in Heat and Mass Transfer*, edited by U. Grigull, and E. Hahne, Vol. 1, Pergamon, London, 1969, pp. 193–329.

[15]Evans, J. S., and Schexnayder, C. J., Jr., "Influence of Chemical Kinetics and Unmixedness on Burning in Supersonic Hydrogen Flames," *AIAA Journal*, Vol. 18, No. 2, 1980, pp. 188–193.

[16]Schultz, D. L., and Jones, T. V., "Heat-Transfer Measurements in Short-Duration Hypersonic Facilities," Dept. of Engineering Science, AGARDograph AGARD-AG-165, Univ. of Oxford, England, UK, 1973.

[17]McIntosh, M. K., "Computer Program for the Numerical Calculation of Frozen and Equilibrium Conditions in Shock Tunnels," Dept. of Physics, School of General Studies, Australian National Univ., Canberra, Australia, 1968.

[18]Lordi, J. A., Mates, R. E., and Morsel, J. R., "Computer Program for the Numerical Solution of Non-Equilibrium Expansions of Reacting Gas Mixtures," NASA CR-472, 1966.

[19]Bittker, D. A., and Scullin, V. J., "General Chemical Kinetics Computer Program for Static and Flow Reactions, with Application to Combustion and Shock-Tube Kinetics," NASA TN D-6586, Jan. 1972.

[20]Huber, P. W., Schexnayder, C. J., Jr., and McLinton, C. R., "Criteria for Self-Ignition of Supersonic Hydrogen-Air Mixtures," NASA TP-1457, 1979.